Modeling of Li-ion Battery Energy Storage Systems (BESSs) for Grid Fault Analysis

Maxime Berger, Ilhan Kocar, Evangelos Farantatos and Aboutaleb Haddadi

***Abstract*— Battery energy storage systems (BESSs) are expected to play a key role in enabling high integration levels of intermittent resources in power systems. Like wind turbine generators (WTG) and solar photovoltaic (PV) systems, BESSs are required to meet grid code requirements during grid disturbances. However, BESSs fundamentally differ from WTG and PV systems because they are not only required to operate as a source (discharging) but also as a load (charging). This paper investigates the system-level behavior of BESSs under grid fault conditions. It presents first a generic electromagnetic transient (EMT)-type model of a two-stage Li-ion BESS that can be configured to comply with grid codes. Compared to previous studies, the proposed model introduces a key step in the characterization of BESSs considering decoupled sequence control (DSC) and the non-linear impact of current limiters under stringent unbalanced faults. The model is used to demonstrate that BESSs behave differently in charging mode, a factor that needs to be accounted in protective relaying practices. The conducted simulations show that the charging mode is more stringent on both dc-link voltage regulation and grid voltage support, and that this is aggravated by the use of DSC scheme compliant with VDE-AR-N 4120 grid code**.

***Index Terms*— Distributed resources, battery energy storage systems, electromagnetic transients, power system protection**

I. Introduction

The increasing integration level of renewable energy resources in power systems, such as wind and solar power, brings new challenges in grid operations due to their intermittent nature. Energy storage systems (ESSs) are key to enable high integration levels of non-dispatchable resources in power systems. While there is no unique solution for storage system technology, battery energy storage systems (BESSs) are highly investigated due to their high energy density, efficiency, scalability, and versatility [1], [2]. Among all the available chemistries, lithium-ion (Li-ion) is currently showing the fastest commercial growth for grid-scale battery storage applications [3].

Similar to wind turbine generators (WTGs) and solar photovoltaic (PV) systems, BESSs fall into the category of inverter-based resources (IBRs) [2], [4]. According to fault ride-through (FRT) requirements of many grid codes, IBRs should support the grid voltage during disturbances and stay connected as specified by voltage versus time curves. IBRs bring a new set of technical challenges related to power system protection because fault currents and voltages exhibit very different characteristics than synchronous generation-based systems [5]. Previous literature has shown that IBRs can lead to mis-operation of protective relays, and that directional elements and negative sequence quantities-based protections are particularly affected by the presence of IBRs [6], [7]. The behavior of IBRs under fault conditions and their impact on protection largely depend on control schemes and local grid code requirements [8]. For example, it has been demonstrated that traditional coupled sequence control (CSC) may have a different impact on power systems protections than decoupled sequence control (DSC) [7].

As WTG and solar PV systems, BESSs are required to meet grid code requirements during grid disturbances [9]. However, in contrast to WTG and PV systems which only operate in inverter mode, BESSs can also operate in rectifier mode for battery charging (Fig. 1) [10]. Historically, rectifier operation was mostly limited to electrical motor drive applications. Therefore, research work was mainly focused on achieving proper control of the dc-link voltage for optimal performance of the electrical motor load under grid fault conditions [11]. However, in addition to dc-link voltage control, BESSs are also required to comply with planning and operation requirements of the grid code, such as grid voltage support and/or negative sequence current injection, in both charging and discharging modes [9]. These fundamental differences of BESSs justify the necessity for proper characterization of their behavior under grid fault conditions considering practical grid code requirements.

While there is a significant amount of research contributions on the short-circuit behavior of WTG- and PV-based systems, the behavior of grid-connected BESSs under fault conditions has not received the same attention in the literature. References [12] and [13] have investigated the impact of BESS on protection for specific systems but without discussing critical details regarding the BESS control systems such as operating mode, type of control and grid code requirements. While [14] and [15] discussed some of these details, the dc-link dynamic is not analyzed, and the analysis is limited to single-stage topology and the use of CSC during FRT. As demonstrated in this paper, both the two-stage

M. Berger and I. Kocar are with the Department of Electrical Engineering, Polytechnique Montreal (Quebec), Canada; E. Farantatos and A. Haddadi with EPRI, USA (e-mails: maxime.berger@polymtl.ca, ilhan.kocar@polymtl.ca, efarantatos@epri.com, ahaddadi@epri.com)

Paper submitted to the International Conference on Power Systems Transients (IPST2021) in Belo Horizonte, Brazil June 6-10, 2021.

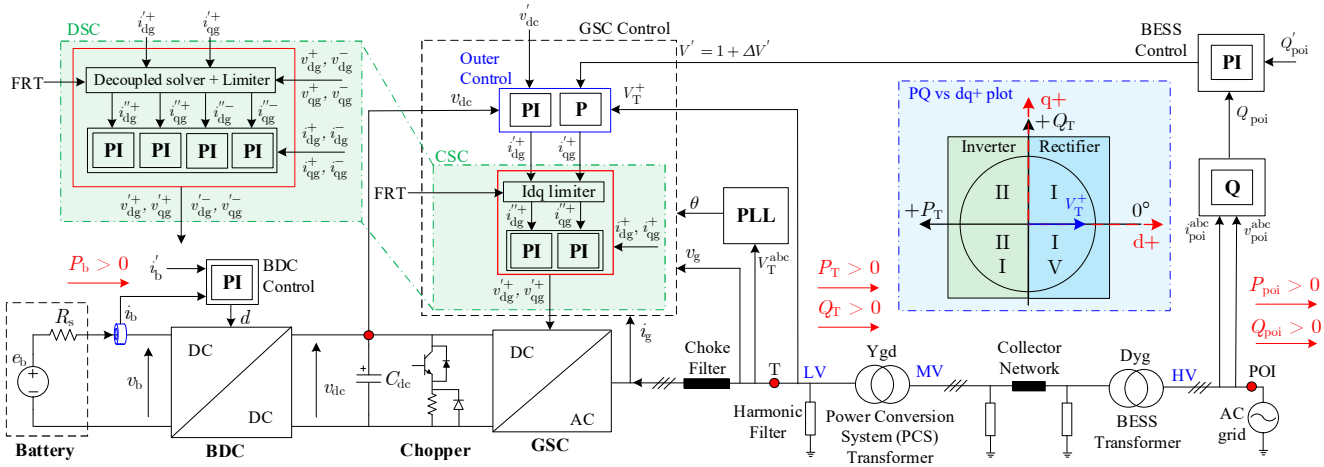

Fig. 1. Simplified schematic diagram of the BESS model.

topology [16] and the use of DSC introduce additional constraints that must be considered in short-circuit analysis of BESSs. Furthermore, it is shown that the dc-link dynamic needs to be analyzed to confirm that BESSs can both ride through faults and comply with grid code requirements in charging and discharging modes.

To enable high integration level of storage in power systems, it is necessary to perform interconnection studies covering a large spectrum of power systems phenomena. Detailed electromagnetic transient (EMT) models including dc-link dynamics, grid-side converter (GSC) controls and FRT strategies offer the highest accuracy for large signal assessments. To the best of the authors' knowledge, there is currently no generic EMT-type model of BESS which includes such level of details.

In response to these challenges, this paper proposes a generic EMT-type averaged value model (AVM) of a two-stage Li-ion BESS that can be configured to comply with grid codes for performing grid-level protection studies. It includes detailed models of Li-ion battery, bidirectional dc-dc converter (BDC) and GSC, as well as generic control schemes, including control system current limiters (Fig. 1). By using the proposed model, this paper characterizes the short-circuit behavior of two-stage BESSs under: 1) different operating modes, i.e. charging and discharging, 2) different type of FRT strategies, such as traditional CSC, and the recent DSC scheme compliant with the VDE-AR-N 4120 Technical Connection Rules [17], which requires injection of additional negative sequence reactive current.

This paper is organized as follows. In section II, the development of the generic AVM Li-ion BESS model is presented with emphasis on model aggregation and control systems. In Section III, the developed BESS AVM is validated with a detailed model (DM), and then the AVM is used to investigate the behavior of BESSs under grid faults with state-of-the-art FRT strategies.

II. Li-Ion Battery Energy Storage System Model

A. Overview

A simplified schematic of the complete BESS model is shown in Fig. 1. The Li-ion battery, the BDC and the GSC models are described in the following subsections. The convention used for the active P_T and reactive Q_T power flow at the GSC terminals, and the corresponding dq-frame references are provided in Fig. 1. The model is implemented in the electromagnetic transient program (EMTP) [18].

B. Li-ion battery model

The Li-ion battery model implemented is a modified version of the generic Li-ion battery model developed in [19]. The terminal voltage is first given by,

$$v_b = e_b - R_s \cdot i_b \tag{1}$$

where v_b is the battery terminal voltage, e_b is the battery internal voltage, R_s is the battery internal resistance and i_b is the battery current. The battery internal voltage e_b is calculated by solving the following equation in time-domain,

$$e_b = E_0 - K\frac{q_a}{q_a - M \cdot it} i_b^* - K\frac{q_a}{q_a - it} it + A e^{-B \cdot it} \tag{2}$$

where E_0 is the battery constant voltage, K is the polarization constant, it is the actual battery level of charge, i_b^* is the filtered battery current, A is the exponential zone amplitude, and B is the inverse exponential zone time constant. The constant M is equal to 0.1 in charging mode and is equal to 1.0 when discharging. The generic model is modified such that the available battery capacity q_a is calculated considering Peukert's effect [20],

$$q_a = Q_n \left[Q_n / \left(n \cdot i_b \right) \right]^{\alpha - 1} \tag{3}$$

with Q_n being the nominal battery capacity if discharged during n hours, and α being Peukert's coefficient.

The developed battery model is an aggregated model that can be adjusted depending on the desired nominal battery capacity Q_n and nominal battery voltage V_n. The aggregated battery model parameters are scaled as follows:

$$\begin{aligned} &A = k_A \cdot V_n \; ; \; B = k_{B1} \cdot Q_n + k_{B2} \; ; \; K = k_K \cdot \frac{V_n}{Q_n} \\ &R_s = k_{Rs} \cdot \frac{V_n}{Q_n} \; ; \; E_0 = k_{E0} \cdot V_n \end{aligned} \tag{4}$$

with the constant k_A, k_{B1}, k_{B2}, k_K, k_{Rs} and k_{E0} being used in conjunction with Peukert's coefficient α to best fit the manufacturer's charge and discharge curves.

The nominal battery voltage V_{n} is calculated based on the nominal dc-link voltage V_{dc}, and must be selected such that $v_{\mathrm{b}} < v_{\mathrm{dc}}$ in both charging and discharging modes to ensure correct behavior of the BDC model. The total nominal aggregated battery capacity Q_{n} (in Ah) is scaled using the following equation,

$$Q_{\mathrm{n}} = \left(N_{\mathrm{BESS}} \cdot P_{\mathrm{BESS}}\right) / V_{\mathrm{dc}} \tag{5}$$

with P_{BESS} being the single BESS unit nominal power and N_{BESS} the number of battery units in service. The initial battery power P_{b} is calculated by,

$$P_{\mathrm{b}} = N_{\mathrm{BESS}} \cdot P_{\mathrm{BESS}} \cdot p_0 \tag{6}$$

with p_0 being the initial power set-point of the BDC (in pu).

The initial battery internal voltage E_{b} is function of the initial battery state-of-charge SOC_0 and the calculated battery model parameters in (4). It is calculated as follows:

$$E_{\mathrm{b}} = E_0 - K\frac{Q_{\mathrm{n}}}{Q_{\mathrm{n}} - it(0)}it(0) + Ae^{-B\cdot it(0)} \tag{7}$$

with,

$$it(0) = Q_{\mathrm{n}}\left(1 - \mathrm{SOC}_0/100\right) \tag{8}$$

C. Bidirectional dc-dc converter (BDC)

The BDC interface allows decoupling the battery from the dc-link and controlling the battery charging and discharging current rates [1], [4]. The equivalent schematic of the BDC is shown in Fig. 2. It is based on the buck-boost topology with battery current control as shown in Fig. 1. The AVM of the BDC is obtained by replacing the switches by controlled voltage and current sources using the methodology in [21].

In boost mode, transistor Q2 is always OFF. Transistor Q1 is controlled by pulse width modulation (PWM) with variable duty cycle d. The duty cycle d is calculated by a PI controller with the objective of regulating the battery discharging current i_{b} to follow its reference $i_{\mathrm{b}}^{'}$. The battery is acting as very slowly varying voltage source e_{b} with small resistance R_{s} and the GSC is modeled as an equivalent resistive load R_{g}.

In buck mode, transistor Q1 is always OFF. Transistor Q2 is controlled by PWM with the duty cycle d being also calculated by a PI controller for regulating the battery charging current i_{b}. The battery is acting as a load R_{L} and the GSC is modeled as a current source i_{gsc}.

In steady-state $e_{\mathrm{b}} = E_{\mathrm{b}}$, $v_{\mathrm{b}} = V_{\mathrm{b}}$, $i_{\mathrm{b}} = I_{\mathrm{b}}$, $i_{\mathrm{gsc}} = I_{\mathrm{gsc}}$, $v_{\mathrm{dc}} = V_{\mathrm{dc}}$, $d = D$ and $D^{'} = 1 - D$. As for the aggregated battery model, the aggregated BDC model is initialized at the steady-state operating point based on BESS level information. Knowing the initial battery power P_{b} calculated in (6), the steady-state operating point is obtained. For boost mode, the operating point is obtained as follows:

$$I_{\mathrm{b}} = V_{\mathrm{dc}}\Big/\left(D^{'}R_{\mathrm{g}}\right),\ D^{'} = \left(R_{\mathrm{g}}E_{\mathrm{b}} + \sqrt{\Delta}\right)\Big/\left(2R_{\mathrm{g}}V_{\mathrm{dc}}\right) \tag{9}$$

where,

$$\Delta = \left(R_{\mathrm{g}}E_{\mathrm{b}}\right)^2 - 4R_{\mathrm{g}}R_{\mathrm{s}}V_{\mathrm{dc}}^2,\ \ R_{\mathrm{g}} = V_{\mathrm{dc}}^2\Big/P_{\mathrm{b}} \tag{10}$$

For buck mode, it can be demonstrated that,

$$D = \left(E_{\mathrm{b}} + \sqrt{\Delta}\right)\Big/\left(2V_{\mathrm{dc}}\right) \tag{11}$$

where,

$$\Delta = E_{\mathrm{b}}^2 + 4V_{\mathrm{dc}}R_{\mathrm{s}}I_{\mathrm{gsc}},\ \ I_{\mathrm{gsc}} = P_{\mathrm{b}}\big/V_{\mathrm{dc}} \tag{12}$$

The perturbation and linearization small-signal average modeling technique [22] is then used to determine the BDC transfer functions and determine PI controller gains. The BDC model is summarized with the standard state-space formalism with $\hat{\mathbf{D}} = 0$. In boost mode, it is proposed here to use the following set of vectors of states, inputs, and outputs,

$$\hat{\mathbf{x}}(t) = \begin{bmatrix}\hat{v}_{\mathrm{dc}}(t)\\ \hat{i}_{\mathrm{b}}(t)\end{bmatrix},\ \ \hat{\mathbf{u}}(t) = \begin{bmatrix}\hat{d}(t)\\ \hat{e}_{\mathrm{b}}(t)\end{bmatrix},\ \ \hat{\mathbf{y}}(t) = \begin{bmatrix}\hat{v}_{\mathrm{dc}}(t)\\ \hat{i}_{\mathrm{b}}(t)\end{bmatrix} \tag{13}$$

with the state-matrices calculated as,

$$\hat{\mathbf{A}} = \begin{bmatrix}\dfrac{-1}{R_{\mathrm{g}}C_{\mathrm{dc}}} & \dfrac{D^{'}}{C_{\mathrm{dc}}}\\ \dfrac{-D^{'}}{L_{\mathrm{b}}} & \dfrac{-R_{\mathrm{s}}}{L_{\mathrm{b}}}\end{bmatrix},\ \ \hat{\mathbf{B}} = \begin{bmatrix}\dfrac{-I_{\mathrm{b}}}{C_{\mathrm{dc}}} & 0\\ \dfrac{V_{\mathrm{dc}}}{L_{\mathrm{b}}} & \dfrac{1}{L_{\mathrm{b}}}\end{bmatrix},\ \ \hat{\mathbf{C}} = \begin{bmatrix}1 & 0\\ 0 & 1\end{bmatrix} \tag{14}$$

and in buck mode, the small-signal model is defined by,

$$\hat{\mathbf{x}}(t) = \left[\hat{i}_{\mathrm{b}}(t)\right],\ \ \hat{\mathbf{u}}(t) = \begin{bmatrix}\hat{d}(t)\\ \hat{v}_{\mathrm{dc}}(t)\end{bmatrix},\ \ \hat{\mathbf{y}}(t) = \begin{bmatrix}\hat{i}_{\mathrm{gsc}}(t)\\ \hat{i}_{\mathrm{b}}(t)\end{bmatrix} \tag{15}$$

$$\hat{\mathbf{A}} = \left[\frac{-R_{\mathrm{s}}}{L_{\mathrm{b}}}\right],\ \ \hat{\mathbf{B}} = \begin{bmatrix}\dfrac{V_{\mathrm{dc}}}{L_{\mathrm{b}}} & \dfrac{D}{L_{\mathrm{b}}}\end{bmatrix},\ \ \hat{\mathbf{C}} = \begin{bmatrix}D\\ 1\end{bmatrix} \tag{16}$$

The transfer functions between the battery current $\hat{i}_{\mathrm{b}}$ and the duty cycle $\hat{d}$ for both boost and buck modes are extracted from (13)–(16), and the PI controller gains are then determined with classical control theory to obtain a desired phase margin at a given cross-over frequency. Adequate control of BDC is necessary to ensure dc-link stability during fault conditions.

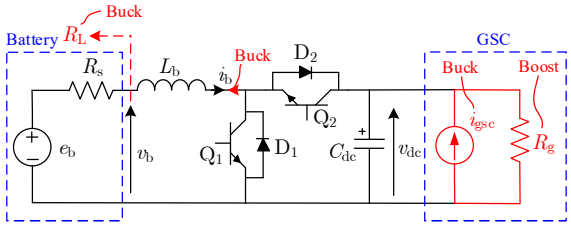

Fig. 2. Bidirectional dc-dc converter (BDC).

D. Grid-side converter (GSC)

According to grid code requirements, the BESS should have a central BESS controller to control reactive power, voltage, or power factor at the point of interconnection (POI), similar to wind park controller (WPC) for wind parks [23]. In this paper, reactive power control is considered, and the output of the BESS controller is a voltage addition $\Delta V^{'}$ (Fig. 1).

The GSC regulates the dc-link voltage v_{dc} through calculation of the d-axis reference current $i_{\mathrm{dg}}^{'+}$. The GSC also controls the positive sequence ac terminal voltage V_{T}^{+} through the q-axis reference current $i_{\mathrm{qg}}^{'+}$ calculated as,

$$i_{qg}^{'+} = K_{V+} \cdot (1 + \Delta V' - V_T^+) \tag{17}$$

with K_{V+} being the positive sequence voltage regulator gain, and $\Delta V'$ the output of the BESS controller. During normal operation, the limiter gives priority to the d-axis (active) current. The outer control logic is the same for both CSC and DSC. However, the sequence and inner controls differ depending on whether CSC or DSC is used. A simplified comparison of CSC and DSC controls is shown in Fig. 1.

Under CSC, the GSC regulates i_{dg}^+ and i_{qg}^+. During fault, priority is given to the q-axis current i_{qg}^+ for grid voltage support. The d- and q-axis currents can be fully regulated as long as the limits defined in [8] are not exceeded.

Under DSC compliant with [17], the GSC is required to inject additional negative sequence reactive current i_{qg}^- to reduce the negative sequence voltage by consuming negative sequence reactive power [23]. The control system uses decoupled double synchronous reference frame (DDSRF) to extract positive- and negative-sequence components in the dq frame [24]. During unbalanced voltage perturbation, the negative sequence reactive current i_{qg}^- is controlled to be proportional to the negative sequence voltage at the GSC terminal V_T^-,

$$i_{qg}^{'-} = K_{V-} \cdot V_T^- \tag{18}$$

with $K_{V-} = 2 \ldots 6$ according to [17]. The positive sequence reactive reference current $i_{qg}^{'+}$ is still calculated using (17). As defined in [8], the reactive reference currents are limited when $\left| i_{qg}^{'+} + i_{qg}^{'-} \right| > I_{qg}^{\lim}$ with,

$$\begin{aligned} i_{qg}^{''+} &= i_{qg}^{'+} \left[I_{qg}^{\lim} \Big/ \left| i_{qg}^{'+} + i_{qg}^{'-} \right| \right] \\ i_{qg}^{''-} &= i_{qg}^{'-} \left[I_{qg}^{\lim} \Big/ \left| i_{qg}^{'+} + i_{qg}^{'-} \right| \right] \end{aligned} \tag{19}$$

where $i_{qg}^{''+}$ and $i_{qg}^{''-}$ are the revised positive and negative sequence reactive reference currents of the GSC. They both have the same priority level over $i_{dg}^{''-}$ and $i_{dg}^{''+}$.

The revised negative sequence active reference current $i_{dg}^{''-}$ is calculated to ensure that the negative sequence current vector $\mathbf{I}_g^-$ is ideally 90° phase-shifted from $\mathbf{V}_T^-$ such that the GSC absorbs purely reactive power in the negative sequence frame. The positive sequence active reference current $i_{dg}^{'+}$ is still calculated by the dc-link voltage outer loop but its revised value $i_{dg}^{''+}$ has a lower priority over $i_{dg}^{''-}$.

III. Case Study

A. Test system

The single-line diagram of the 120 kV test system is shown in Fig. 3. The aggregated BESS model is composed of $N_{BESS} = 45$ single BESS units of $P_{BESS} = 1.5$ MW. The dc-link voltage is regulated at $V_{dc} = 1$ pu by the GSC. The BESS controller is controlling the reactive power absorbed at the POI at $Q_{poi}' = -0.1$ pu. At $t = 3$ s a double line to ground fault is applied at BUS4 (distant fault). The fault duration of one second is not practical, i.e. it is too long, but selected to clearly show the transient and steady-state responses of the controllers in the figures.

B. Average Value Model (AVM) vs Detailed Model (DM)

The AVM of the BESS is validated with the DM in charging mode under DSC control. The BDC is operated at $p_0 = 0.5$ pu. The battery charging current is regulated by the BDC at $i_b = -0.5$ pu. For AVM, the time-step $\Delta t = 50$ μs and for DM $\Delta t = 5$ μs.

The resulting GSC reference currents are shown in Fig. 4. From these results, it is concluded that the BESS AVM is accurate for grid-level fault studies. The small difference on the positive sequence active current during fault is due to small losses within the non-linear IGBTs/diodes of the BDC and GSC converters with DM. Low frequency oscillations are due to PLL transient response at fault inception and fault removal. PLL response is beyond the scope of this paper.

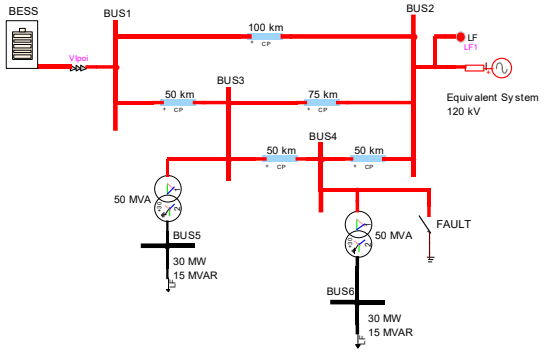

Fig. 3. 120 kV/60 Hz test system.

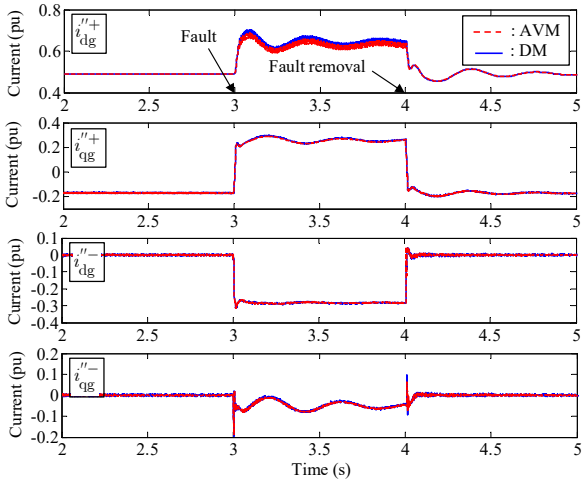

Fig. 4. Reference currents for AVM and DM in charging mode with DSC. The current i_{dg}^+ is higher with DM because losses within the GSC and BDC are supplied by the grid. Conversely, in discharging mode, i_{dg}^+ is lower with DM because losses are supplied by the battery rather than GSC (not shown).

C. Behavior of BESS under fault

The impacts of the BESS operating mode (charging vs discharging) and control type (CSC vs DSC) under fault conditions are investigated here. The results are shown in Fig. 5 to Fig. 8. The grid side results are summarized by the phasor diagrams in Fig. 9. The results are analyzed below.

From Fig. 5 and Fig. 6, it is first observed that the operating mode (charging vs discharging) has an important impact on dc-link transient voltage v_{dc}. From Fig. 6, it is also noted that, for higher active power transfer, the use of DSC compliant with [17] highly affects the dc-link dynamic for the same fault.

By comparing Fig. 7 and Fig. 8, it is observed that the required negative sequence injections i_{qg}^{-} and i_{dg}^{-} are nearly independent of the active power flow level p_0 in both charging and discharging modes. However, the amount of i_{dg}^{+} that is required by the GSC to maintain a constant dc-link voltage v_{dc} is highly dependent on p_0. Since i_{dg}^{+} has the lowest priority during FRT, the GSC ability to regulate the dc-link voltage is affected by the levels of i_{qg}^{-}, i_{qg}^{+} and i_{dg}^{-}.

Therefore, as seen by analyzing Fig. 6 and Fig. 8, in discharging mode, if i_{dg}^{+} cannot be fully regulated by the GSC, steady-state overvoltage occurs on the dc-link and the chopper must dissipate the excess of power on the dc-link. In charging mode, if i_{dg}^{+} cannot be fully regulated by the GSC, undervoltage occurs on the dc-link and the BDC is not capable of regulating the battery charging current i_b. In this case, the BDC current controller saturates, which may prevent the BESS from meeting FRT and grid code requirements. The transient and steady voltage drops observed on the dc-link are also function of the battery internal voltage and internal resistance at fault inception (not shown). These results suggest that the BDC should reduce its charging or discharging current to allow proper regulation of the dc-link voltage during FRT. Investigation of alternative solution strategies is not covered here due to space constraints.

Furthermore, from Fig. 7 and Fig. 8, it is noted that the required injection of i_{dg}^{-} with DSC is higher in charging mode than in discharging mode, which means that the effort in the d-axis to keep $\mathbf{I}_g^{-}$ at 90° from $\mathbf{V}_T^{-}$ is higher in charging mode (Fig. 9). Therefore, for a limiter logic which gives priority to i_{dg}^{-} over i_{dg}^{+}, charging mode can be more stringent on dc-link voltage regulation.

Additional results provided in Fig. 10 also show that the charging mode is more demanding on ac grid voltage support due to voltage drops caused by active power consumption of the BESS in charging mode during fault (i_{dg}^{+} is positive in Fig. 9). Furthermore, DSC tends to be more stringent on grid voltage support because i_{qg}^{+} is limited by the required injection of i_{qg}^{-}. However, at power close to $p_0 = 1$ pu, CSC is more restrictive in charging mode because i_{dg}^{+} is not limited by any injection of negative sequence currents.

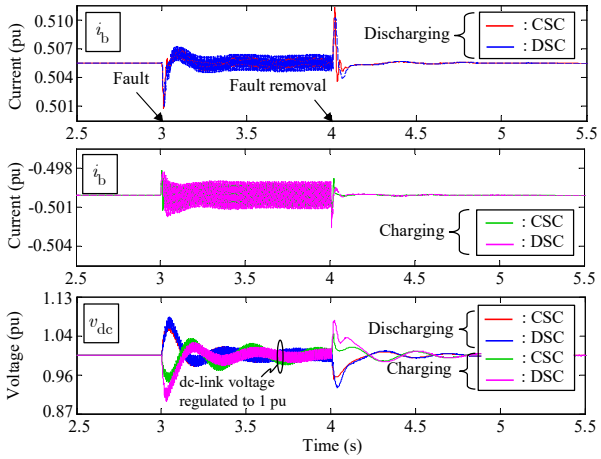

Fig. 5. Battery current and dc-link voltage for $p_0 = 0.50$ pu

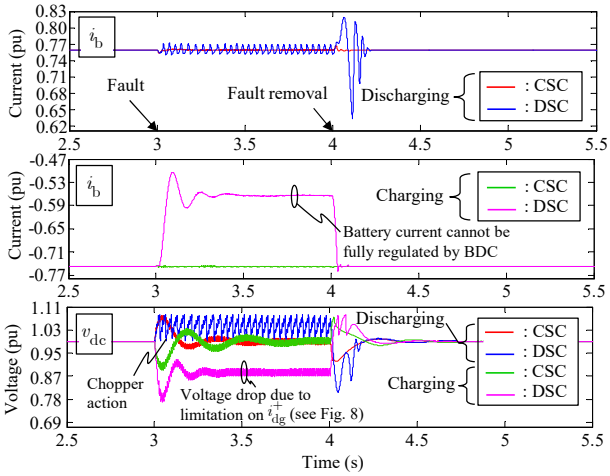

Fig. 6. Battery current and dc-link voltage for $p_0 = 0.75$ pu.

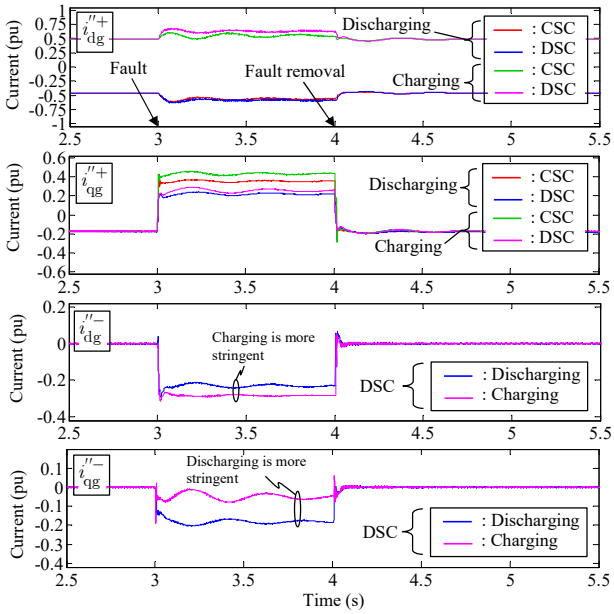

Fig. 7. GSC reference currents for $p_0 = 0.50$ pu.

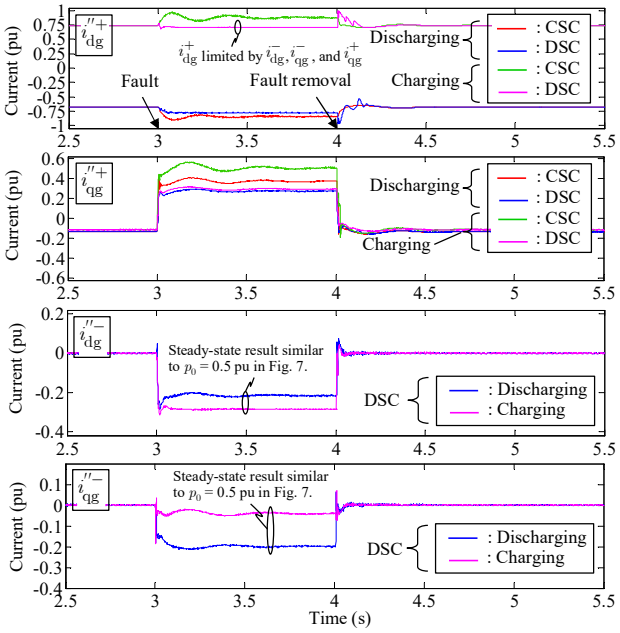

Fig. 8. GSC reference currents for $p_0 = 0.75$ pu.

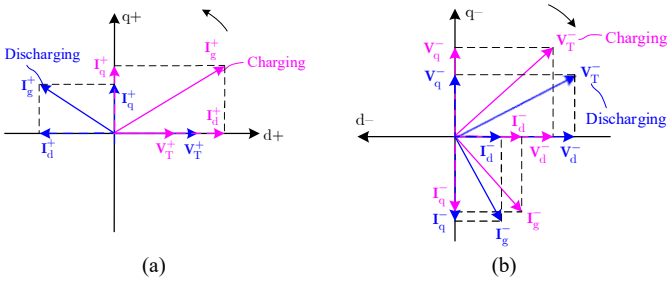

Fig. 9. Phasor diagrams of voltage and current at GSC terminals. (a) positive sequence frame, (b) negative sequence frame (DSC)

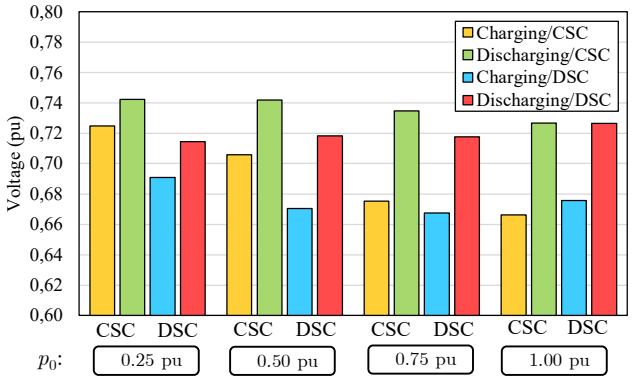

Fig. 10. Voltage at the POI calculated by the BESS controller

IV. Conclusion

This paper is a key step forward towards describing the behavior of grid-connected BESS under grid fault conditions, and the stress on dc-voltage regulation and ac grid voltage support considering practical grid code requirements. The successful integration of BESSs in power systems requires accurate characterization of their behavior during fault conditions and tuning of their controllers based on grid codes.

In this paper, a generic EMT-type AVM of two-stage BESS is presented. The developed model is used to demonstrate that BESSs behave differently depending on whether they are operated in charging or discharging mode at fault inception. Furthermore, through comparisons of the behavior with CSC and DSC compliant with [17] schemes, under both charging and discharging modes, it is shown that the impact of DSC on BESS operation is more stringent in charging mode compared to discharging mode.

V. References

[1] Fu-Bao Wu, B. Yang, and Ji-Lei Ye, *Grid-scale Energy Storage Systems and Applications*, Academic Press, 2019, p. 1-15.

[2] M. T. Lawder et al., "Battery energy storage system (BESS) and battery management system (BMS) for grid-scale applications," *Proc. IEEE*, vol. 102, no. 6, pp. 1014–1030, Jun. 2014.

[3] B. M. Grainger, G. F. Reed, A. R. Sparacino, and P. T. Lewis "Power electronics for grid-scale energy storage," *Proc. IEEE*, vol. 102, no. 6, pp. 1000–1013, Jun. 2014.

[4] *IEEE Guide for Design, Operation and Maintenance of Battery Energy Storage Systems, both Stationary and Mobile, and Applications Integrated with Electric Power Systems*, IEEE Std 2030.2.1, Dec. 2019.

[5] "Impact of inverter-based generation on bulk power system dynamics and short-circuit performance", PES-TR68, prepared by the IEEE/NERC Task Force on Short-Circuit and System Performance Impact of Inverter Based Generation, Jul. 2018.

[6] A. Hooshyar, M. A. Azzouz, and E. F. El-Saadany, "Distance protection of lines emanating from full-scale converter-interfaced renewable energy power plants–Part I: Problem statement," *IEEE Trans. Power Del.*, vol. 30, no. 4, pp. 1770–1780, Aug. 2015.

[7] A. Haddadi, M. Zhao, I. Kocar, U. Karaagac, K. W. Chan, and E. Farantatos, "Impact of Inverter-Based Resources on Negative Sequence Quantities-Based Protection Elements," *IEEE Trans. Power Del.,* March 2020 [Early Access].

[8] U. Karaagac et al., "A generic EMT-type model for wind parks with permanent magnet synchronous generator full size converter wind turbines," *IEEE Power and Energy Tech. Syst. J.*, vol. 6, no. 3, pp. 131–141, Sep. 2019.

[9] *IEEE Standard Test Procedures for Electric Energy Storage Equipment and Systems for Electric Power Systems Applications*, IEEE Std 2030.3-2016, Sep. 2016.

[10] *IEEE Recommended Practice for the Characterization and Evaluation of Energy Storage Technologies in Stationary Applications*, IEEE Std 1679-2020, Apr. 2020.

[11] R. Teodorescu, M. Liserre, and P. Rodriguez, *Grid Converters for Photovoltaic and Wind Power Systems*. Hoboken, NJ, USA: Wiley, 2011.

[12] F. M. Gatta et al., "Modelling of battery energy storage systems under faulted conditions: Assessment of protection systems behaviour," *IEEE Int. Conf. Env. and Elect. Eng. (EEEIC)*, June 2016, pp. 1–6.

[13] A. Neves et al., "Protection scheme for energy storage systems operating in island or grid-connected modes," *CIRED - Open Access Proc. J.*, vol. 2017, no. 1, pp. 1384–138.

[14] Y. Bak, J.-S. Lee, and K.-B. Lee, "A low voltage ride through control strategy for energy storage systems," in *Proc. Energy Convers. Congr. Expo. (ECCE)*, Milwaukee, WI, USA, Sep. 2016, pp. 1–6.

[15] H. Wang, Q. Zhang, D. Wu, and J. Zhang, "Advanced Current-Droop Control for Storage Converters for Fault Ride-Through Enhancement," in *IEEE J. Emerg. Sel. Topics Power Electron.*, vol. 8, no. 3, pp. 2461–2474, Sep. 2020.

[16] S. Vazquez, S.M. Lukic, E. Galvan, L. G. Franquelo, and J. M. Carrasco, "Energy Storage Systems for Transport and Grid Applications", *IEEE Trans. Ind. Electron.*, vol. 57, no. 12, pp. 3881–3895, Dec. 2010.

[17] *Technische Regeln den Anschluss von Kundenanlagen an das Hochspannungsnetz und Deren Betrieb (TAR Hochspannung), VDE-AR-N 4120 Anwendungsregel*, Oct. 2018.

[18] J. Mahseredjian, S. Dennetiere, L. Dube, B. Khodabakhchian, and L. Gerin-Lajoie, "On a new approach for the simulation of transients in power systems," *Electr. Power Syst. Res.*, vol. 77, no. 11, pp. 1514–1520, Sep. 2007.

[19] O. Tremblay and L.-A. Dessaint, "Experimental validation of a battery dynamic model for EV applications," *World Electr. Veh. J.*, vol. 3, no. 1, pp. 1–10, 2009.

[20] D. Doerffel and S.A. Sharkh "A critical review of using the Peukert equation for determining the remaining capacity of a lead-acid and lithium-ion batteries," *Journal of Power Sources*, vol. 155, iss. 2, pp. 395–400, 2006.

[21] R. D. Middlebrook and S. Cùk, "A general unified approach to modelling switching-converter power stages," in *Proc. IEEE Power Electron. Spec. Conf.*, pp. 18–34, June 1976.

[22] R. W. Erickson and D. Maksimovic, *Fundamental of Power Electronics*. 2nd ed., Norwell, MA, USA: Kluwer, 2001.

[23] T. Kauffmann et al., "Short-circuit model for type-IV wind turbine generators with decoupled sequence control," *IEEE Trans. Power Del.*, vol. 34, no. 5, pp. 1998–2007, Oct. 2019.

[24] P. Rodrigue, J. Pou, J. Bergas, J. I. Candela, R. P. Burgos, and D. Boroyevich, "Decoupled double synchronous reference frame PLL for power converters control," *IEEE Trans. Power Electron.*, vol. 22, no. 2, pp. 584–592, Mar. 2007.